Improved Streamflow Simulations in Hydrologically Diverse Basins using Physically Informed Deep Learning Models

Bhanu Magotra[a], Manabendra Saharia[a,b*], C.T. Dhanya[a]

a Department of Civil Engineering, Indian Institute of Technology Delhi, Hauz Khas, New Delhi 110016, India

b Yardi School of Artificial Intelligence, Indian Institute of Technology Delhi, Hauz Khas, New Delhi 110016, India

Corresponding Author:

Dr. Manabendra Saharia

Assistant Professor

Indian Institute of Technology Delhi

New Delhi, India 110016

Office: +91-011-26591260

Email: msaharia@iitd.ac.in

Note: This manuscript has been peer reviewed and accepted for publication in Hydrological Sciences Journal.

Improved Streamflow Simulations in Hydrologically Diverse Basins using Physically Informed Deep Learning Models

Physically informed deep learning models, especially Long Short-Term Memory (LSTM) networks, have shown promise in large-scale streamflow simulations. However, an in-depth understanding of the relative contribution of physical information in deep learning models has been missing. Using a large-sample testbed of 220 catchments in hydrologically diverse regions of the Indian subcontinent, we quantify the impact of incremental addition of physical information on model performance using multiple variants of the LSTM model based on various combinations of static catchment attributes and simulated land surface states. We found that LSTM models trained with catchment geophysics as additional input outperformed the base LSTM model in terms of the nationwide median Kling-Gupta Efficiency (KGE) of in-sample catchments, increasing KGE from 0.32 to 0.60. Additionally, the model retained significant prediction skill in out-of-sample catchments, demonstrating that a pre-trained LSTM model can be a powerful tool to predict streamflow in data-scarce regions.

Keywords: LSTM, deep learning, streamflow, physically informed models, large-sample hydrology.

1 Introduction

Efficient water resource management necessitates the utilization of precise and reliable data. Streamflow data is essential for determining water availability and assessing the impact of water usage on the environment. It is also crucial for assessing the streamflow variability over time and space and predicting future water availability. To make informed decisions, policymakers need to have access to the most accurate streamflow estimates possible. The estimation of streamflow begins with attempts to model the naturally occurring processes involved in rainfall-runoff generation using mathematical equations of varying complexities. These mathematical models are known as hydrological models, which can be categorized as empirical, conceptual, and physically based (Devia et al., 2015). The hydrological models have been progressively improved in process representation along with increasing spatial and temporal resolution of the frameworks that are used to run these models (Burnash et al., 1973; Ek et al., 2003; Lawrence et al., 2019; Liang et al., 1994; Niu et al., 2011). However, these models require intensive calibration of the parameters, which is a time-consuming, complex, and computationally expensive process (Arsenault et al., 2014; Hirpa et al., 2018; Yucel et al., 2015). In contrast to physically based hydrological models that involve explicit representations of land-atmosphere interactions, data-driven methods have been developed that use statistical learning to map the relationship between a set of independent variables like meteorological forcings and a target variable such as streamflow, which makes them easier to implement and faster to run than physically based models. With advancements in computation and data availability, the multi-layered deep learning networks have become popular as they can leverage large volumes of data to learn intrinsic relationships among various processes that are difficult to represent otherwise (Solomatine and Ostfeld, 2008; Young and Beven, 1994).

The earliest applications of advanced data-driven modelling involved Artificial Neural Networks (ANNs) that used a combination of deeply connected feed-forward layers of weights

and parameters enabling the modelers to capture complex non-linear dynamics of land-atmosphere interactions (Govindaraju, 2000; Hsu et al., 1995; Minns and Hall, 1996). However, ANNs were agnostic to temporal patterns and hence failed to capture the long-term dependencies of hydrological data and, thus, were limited in terms of the accuracy of data-driven models. The Recurrent Neural Networks (RNNs), with the introduction of a feedback mechanism, enabled the passing of information between timesteps, which enabled RNNs to retain information about past inputs and incorporate it into current predictions (Chang et al., 2003; Coulibaly et al., 2000; Parlos et al., 2000; Rumelhart et al., 1986). While RNNs could capture some of the temporal dependencies in the data, they were subject to the problem of vanishing or exploding gradients over a longer length of temporal data during training (Bengio et al., 1994). This drawback inhibited their adoption for rainfall-runoff modelling as the hydrological processes often possess very long-term dependencies that may exist over a span of multiple months. To overcome this problem, a new state-of-the-art deep learning technique, known as the Long Short-Term Memory (LSTM) network model was introduced, which could utilize memory cells, input gates, forget gates, and output gates, which help control the flow of information through time and mitigate the vanishing/exploding gradient problem (Hochreiter and Schmidhuber, 1997). The memory cells enable LSTM networks to retain and selectively forget information over extended intervals, making them highly effective in capturing long-term dependencies. Kratzert et al. (2018) successfully trained LSTM based models on catchments in Conterminous United States (CONUS) using CAMELS (Addor et al., 2017) dataset to capture rainfall-runoff dynamics. In recent years, many studies have been carried out involving various augmentations of LSTM models to predict various hydrological applications, including streamflow (Lees et al., 2021; Ni et al., 2020; Xiang et al., 2020), flood forecasting (Kao et al., 2020), sediment load (Wang et al., 2019), soil moisture (Fang and Shen, 2020), and so on. Additionally, efforts have been made to explore the capabilities of LSTM models to learn generalized patterns across spatial domains so that the skill of the model could be

transferred to un-seen catchments (Kratzert et al., 2019). Historically observed streamflow is relatively sparse and the record length also varies significantly in India. Consequently, very few studies have explored the potential of deep learning based hydrological models in India. A few of the studies have been conducted over a single basin which limits their applicability for large-scale modelling (Khatun et al., 2023; Sahoo et al., 2019; Yeditha et al., 2021). A recent study has explored modeling LSTM under various settings, such as individual catchment models vs a collective model, performance in gauged vs ungauged basins, and data-integration with lagged observations on 55 catchments across peninsular and southern India (Mangukiya et al., 2023). While the study has made valuable contributions to the data-driven hydrological modeling in India, it should be noted that their analysis is based on a relatively small sample of 55 catchments, which further reduces to 36 for gauged vs ungauged experiments, excluding a considerable potential out of LSTM models for large sample hydrological modelling. E.g., studies by Kratzert et al. in United States of America and Lees et al. in Great Britain were conducted using a large sample dataset of 221 and 669 catchments, respectively, highlighting that models have been found to excel when a large number of training samples are available, resulting in a broader real-world application with more reliable predictions. Hestness et al., (2017) also demonstrated that deep learning models trained in a "small data region" generally perform at a level comparable to random guessing. Moreover, studies have shown that LSTM models can utilize similarities between catchments when trained on a large dataset, allowing for effective information transfer across basins and significantly improving performance in ungauged basins (Kratzert et al., 2024; Nearing et al., 2021). Therefore, in this study, a concerted effort was made to include a substantially large training dataset to develop a robust data-driven streamflow prediction model.

In this study, we have attempted to address two key research questions. First, we examine the relative contribution of geophysical catchment attributes and simulated land surface outputs from a physically based model in improving the skill of the LSTM model. We

trained the LSTM network with two distinct sets of physical information in addition to the commonly used meteorological variables in the training data: a) static attributes that represent various geophysical characteristics of the catchments, and b) dynamic land surface states simulated using a high resolution fully distributed physically based model. Second, we present an overall assessment of potential application of physically informed machine learning in large-scale hydrological modelling in India. In regions where historical observations are limited, training of deep learning models may be enhanced using additional data such as geophysical attributes and simulated land surface states. To understand whether the performance of such physically informed LSTM models, observed in multiple global studies, translates to Indian catchments, we tested multiple LSTM variants on 220 catchments across India, including the basins in northern and central India using different sets of training data (see section 2.1). We conducted an objective assessment of model performance based on various error metrics and hydrological signatures. We also examined the difference in model skills based on the effect of human influence and climate of the region. Moreover, we also evaluated the model in an ungauged setting to better understand its performance in a national-scale operational framework where streamflow predictions are needed across all catchments, both gauged and ungauged. We trained the LSTM models that learn to simulate the observed streamflow using different sets of training inputs over a group of 170 catchments out of a total 220. The remaining 50 were not used in training the models and were considered as an out-of-sample dataset used only for testing the results in "ungauged" conditions.

The paper is organized as follows: section 2 describes the datasets used in this study. It also briefly explains the LSTM model and the methodology involved in running the model and the evaluation of the results. In section 3, results are presented along with relevant discussion. Finally, section 4 provides the conclusions of the study and future work.

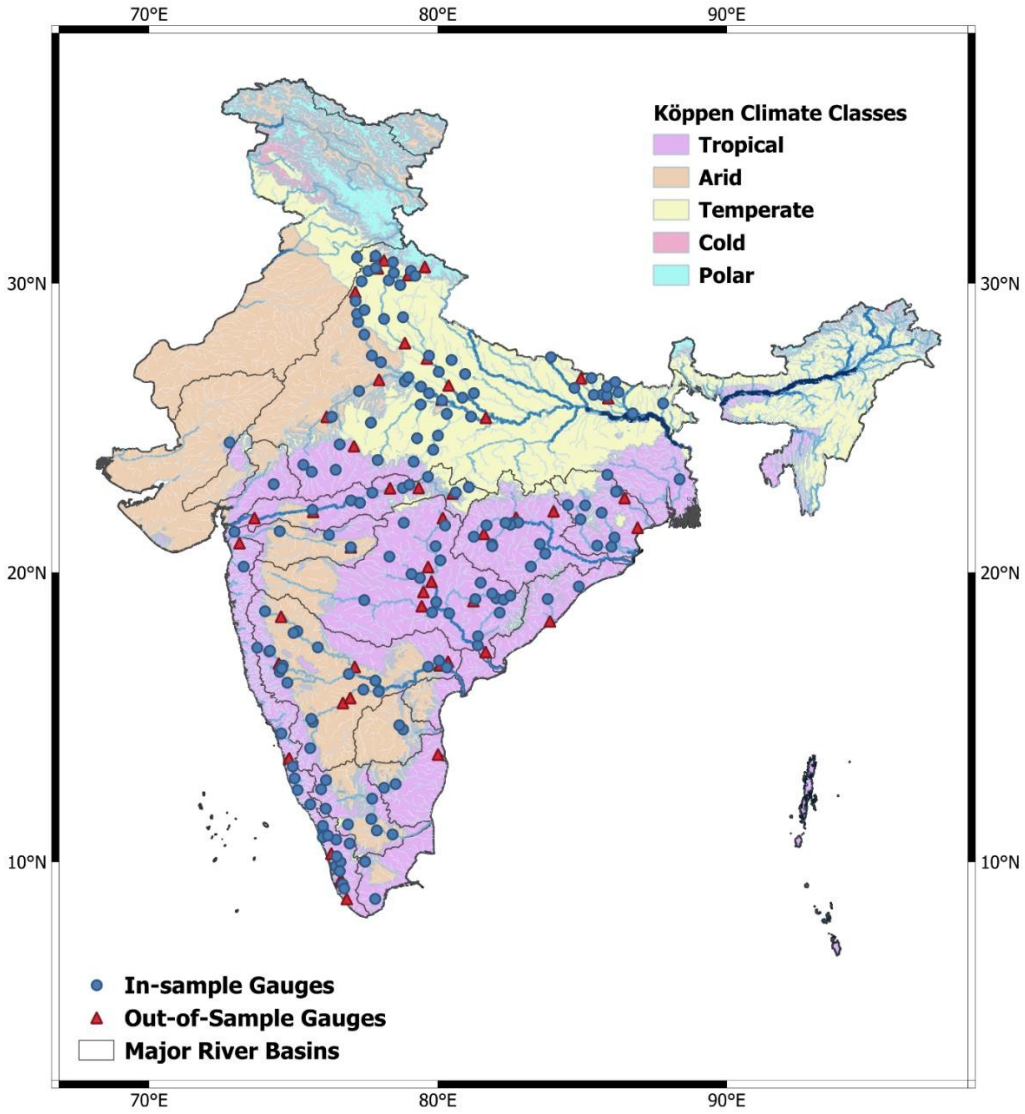

Figure 1. A map of India showing the location of streamflow gauge points, major river basins and Köppen-Geiger climate classes considered in the study.

2 Data and methods

We start with an LSTM model that learns to map dynamic meteorological forcing variables to the observed streamflow by training over 170 catchments out of 220 in the training dataset. The remaining 50 were not used in training the models and were considered as an out-of-sample dataset used only for testing the results in “unseen” conditions. In the second experiment, we provide simulated physics-based information through dynamic land surface states generated by Noah-MP3.6 land surface model. We wanted to test the hypothesis that incorporating dynamic

physics-based information should enable the data-driven model to better understand the processes behind catchment hydrology, thus becoming process-aware and improving the streamflow simulations. Our third LSTM model leverages auxiliary information in the form of static catchment attributes, which may help it learn similarities between different catchments, resulting in a robust and transferable catchment-aware model. In our fourth model, we provide both land surface states and catchment attributes together to see if the model gains any additional skill. We evaluated the relative gain (or loss) in the skill by using Kling-Gupta Efficiency Skill Score (KGESS). Additionally, we calculated various error metrics and hydrological signatures that provide important insights towards the suitability of LSTM model across a relatively sparse and highly varying hydrological domain such as India. Fig.2 represents the complete methodology adopted in this study.

2.1 Dataset

The dataset consists of 220 gauge locations in the Indian mainland, where daily recorded streamflow observations were available for at least 20 years. The daily streamflow observed records were collected from various government agencies through the public domain and official requests. The records were checked for data inconsistencies and were converted to a standard format for analysis. Considering each gauge station as a pour-point, we programmatically delineated the watersheds using a high-resolution digital elevation model (DEM). Due to varying record lengths across the catchments, the training, validation, and testing periods were uniquely specified for each basin. Additionally, to assess the generalizability of the model, we randomly sampled 50 catchments that were exclusively used for evaluation of model performance in out-of-sample conditions, implying that the models were not trained on them but only tested (Fig.1). Along with the streamflow observations, the dataset also included 7 daily meteorological forcings timeseries and 19 static attributes derived from various sources that were averaged over each catchment (Annexure 1). The precipitation

and related variables were derived from the 0.25º daily gridded dataset provided by the Indian Meteorological Department (IMD, Pai et al., 2014). Similarly, temperature-based characteristics were derived using IMD's gridded 1º daily temperature data (Srivastava et al., 2009). The rest of the meteorological variables were averaged over the catchments using Indian Monsoon Data Assimilation and Analysis (IMDAA, Rani et al., 2021). We used Multi-Error-Removed Improved-Terrain DEM (MERIT DEM, Yamazaki et al., 2017) for elevation and related variables. The soil properties were derived from SoilGrids (Hengl et al., 2017) and HiHydroSoil v2.0, which are available as 250-m global raster datasets. Additionally, we used Moderate Resolution Imaging Spectroradiometer Leaf Area Index (MODIS LAI, Myneni, Ranga et al., 2021) and ERA5 evapotranspiration (Hersbach et al., 2020) datasets. The land use and land cover properties of the catchments were extracted programmatically using the python-based raster analysis from the National Remote Sensing Centre (NRSC) LULC 56m dataset. Since deep learning possesses the capabilities for end-to-end modelling, we did not perform an initial stage feature selection, and let the model naturally uncover the correlations between the features and target streamflow.

Additionally, we set up a 3-member ensemble of a hydrologic-hydrodynamic model (Noah-MP3.6 + HyMAP2) which was run at 0.1° daily over the South-Asia domain spanning from 68°E – 98°E and 5.5°N – 37.5°N from 1980-2021. Each member of the model was forced with a different global precipitation source (Chakraborty et al., 2024; Magotra et al., 2022). The model provided high-resolution water balance components and energy fluxes in gridded outputs. Since the model is physically based, we used the simulated land surface states as a proxy for the catchment hydrological processes. The catchment-averaged timeseries for three simulated variables were selected, namely: soil moisture, surface runoff and baseflow.

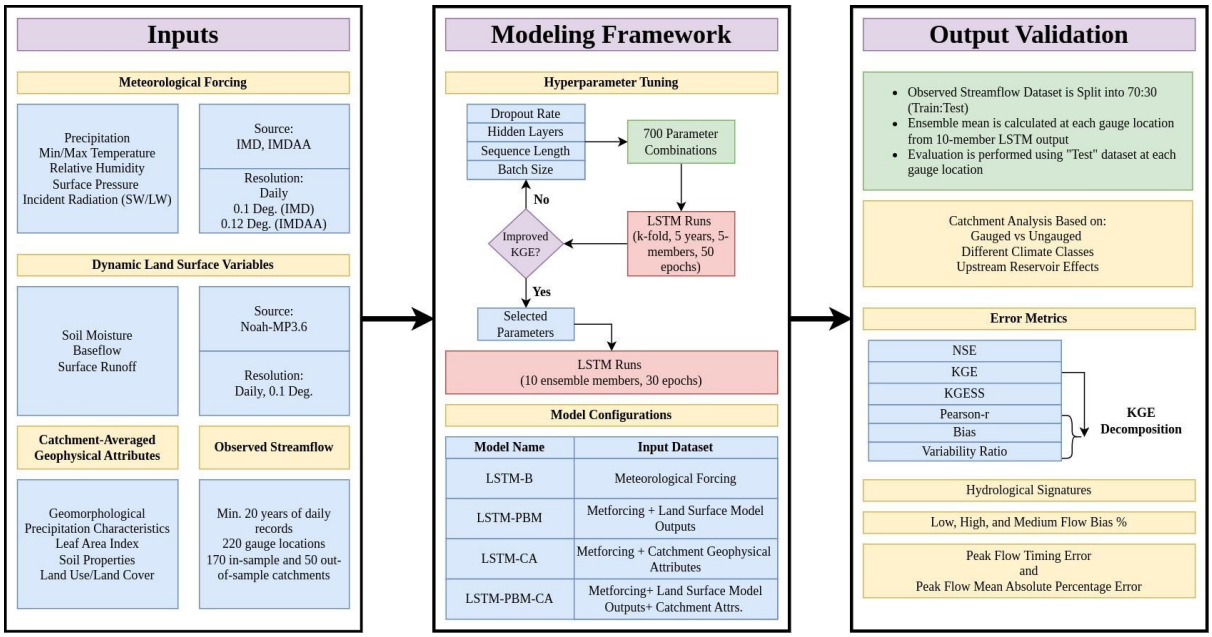

Figure 2. Methodology adopted in this study.

2.2 Modeling framework

2.2.1 Long Short-Term Memory Network

LSTM networks are a modification of RNNs first introduced by Hochreiter and Schmidhuber (1997). LSTM networks were designed to avoid the problems of exploding or vanishing gradients as present in existing forms of RNNs. This allowed LSTM networks to learn the temporal patterns which were present on a longer timeline, such as vegetation seasonality, snowmelt, groundwater dynamics, and so on. To retain the past information of a time series, LSTM networks employ memory cells that are like system states in a typical dynamic model. The model takes a sequence of inputs, ordered in the form of a timeseries, x = [x1, .., xT] of data over T time steps, where each element xt is a vector containing model inputs as features at time step t. The LSTM model structure can be explained using the following equations: where each element xt is a vector containing model inputs as features at time step t. The LSTM model structure can be explained using the following equations:

$$i_t = \sigma(W_i x_t + U_i h_{t-1} + b_i) \qquad (1)$$

$$f_t = \sigma(W_f x_t + Ufh_{t-1} + bf) \quad (2)$$

$$g_t = \tanh\,(Wgx_t + Ugh_{t-1} + bg) \quad (3)$$

$$o_t = \sigma\,(W_o x_t + U_o + b_o) \quad (4)$$

$$c_t = f_t \odot c_{t-1} + i_t \odot g_t \quad (5)$$

$$h_t = o_t \odot \tanh\,(c_t) \quad (6)$$

where it, ft, and ot are the input gate, forget gate, and output gate, respectively, gt is the cell input and xt is the network input at time step t ($1 \le t \le T$), ht−1is the recurrent input and ct−1 the cell state from the previous time step. At the start, the hidden and cell states are initialized as a vector of zeros. W, U, and b are calibrated parameters specific to each gate, as denoted by the subscripts. The architecture involves two activation functions, the sigmoid, σ (·), and the hyperbolic tangent, tanh (·). $\odot$ denotes the element-wise multiplication. The ct acts like the memory of the system which gets altered by the forget gate and a combination of input gate and cell update. The forget gate controls which information needs to be deleted and the input gate with cell update governs the information that needs to be added to the cell state memory. Finally, the output gate controls the flow of information from the cell state to the output layer.

Table 1. Hyperparameters and their values used for hyperparameter tuning. The bold values represent the final selection for training the models.

	Hyper Parameter	***Values***
1	Dropout Rate	[0,0.25,***0.4***,0.5]
2	Hidden Layers	[***64***,96,128,160,192,224,256]
3	Sequence Length	[30,90,180,270,***365***]
4	Batch Size	[64,128,256,***512***,1024]

2.2.2 Model Configuration

Initially, we performed hyperparameter tuning using 50 catchments that were randomly sampled separately from those classified as out-of-sample catchments in section 2.1. We used the k-fold technique to divide the catchments into five sets of equal numbers and performed training on 40 catchments and testing on the remaining 10. We selected four hyperparameters for our experiments, namely dropout rate, number of hidden layers, sequence length, and batch size. The corresponding parameters selected for tuning are shown in Table 1. We trained a 5-member ensemble model for 50 epochs on five years of data split as 3:1:1. Overall, we tested 700 combinations and trained 3500 models. The selection of a hyperparameter value was made using the highest mean ensemble KGE value.

Table 2. Details of four model configurations that were evaluated in the study. Each model is trained using a distinct set of input variables including meteorological data, land surface model outputs, and catchment geophysical attributes.

	Model	***Input Variable***	***Target Variable***
1	LSTM-B	Meteorological	Daily Streamflow
2	LSTM-PBM	Meteorological + Dynamic Land Surface Model Outputs	Daily Streamflow
3	LSTM-CA	Meteorological + Static Catchment Attributes	Daily Streamflow
4	LSTM-PBM-CA	Meteorological + Dynamic Land Surface Model Outputs + Static Catchment Attributes	Daily Streamflow

Table 2. shows the details of the configuration of four LSTM models that were trained using a 10-member ensemble for each model type to account for stochasticity due to randomly initialized weights. Each feature was normalized using zero mean and unit variance, wherein

the time series is first reduced by its mean and then divided by the standard deviation. This allows the DL model to reach optimal solutions without getting biased by features having large values. The models were trained for 30 epochs and a learning rate of 0.001 on 170 catchments simultaneously. We used Nash-Sutcliffe Efficiency (NSE) as the objective function, and optimizations were performed using ADAM optimizer (Kingma and Ba, 2017). In total, we trained and tested 40 models using the same architecture. The LSTM networks had a dropout rate of 0.4 which prevents the overfitting of the model and improves robustness by randomly dropping some weights (40% in our case) to zero. The hidden size was set to 64 with a batch size of 512 and the sequence length of 365 days. The results were evaluated using an ensemble mean of predicted daily streamflow in the testing period and compared against observed streamflow in the same period. We used "NeuralHydrology" python package (Kratzert et al., 2022) to perform the training, validation, and testing of the models. The models were trained on a High-Performance Computer (HPC) facility using Nvidia A100 40GB GPU hosted by the Indian Institute of Technology, Delhi.

2.3 Evaluation criteria

2.3.1 Error Metrics

To evaluate the predictive skill of the models, we selected Nash Sutcliffe Efficiency (NSE) and Kling Gupta Efficiency (KGE; Gupta et al., 2009) as our primary metrics. We also decomposed the KGE into its three components, namely, correlation coefficient (r), variability ratio(α), and bias(β). The three components of KGE highlight different parts of the performance of a model where the agreement between the timing of simulated and observed values is given by correlation (r), the statistical variability is expressed by variability ratio (α), and the bias is highlighted by bias (β). A KGE value equal to 1 (r=1, α=1, β=1) means a perfect agreement between simulated and observed values. These error metrics provide us with an overview of the agreement between the daily observed and simulated time series, specifically focusing on

timing, bias, and variability deviations between the two. To objectively define the increase (or decrease) of skill in the various model configurations, we used Kling Gupta Efficiency Skill Score (KGESS, Hirpa et al., 2018) defined as:

$$KGESS = \frac{KGE_{perf} - KGE_{base}}{1 - KGE_{base}}$$

where KGE_{perf} and KGE_{base} are the catchment-wise KGEs for new and base LSTM models, respectively. In the denominator, the KGE_{base} is subtracted from the highest possible KGE value, i.e., 1. We calculated the KGESS for LSTM-PBM, LSTM-CA, and LSTM-PBM-CA against LSTM-B.

2.3.2 Hydrological Signatures

A set of four commonly used hydrological signatures were derived from observed and modeled daily streamflow to assess LSTM models' ability to capture seasonal trends. The comparison between the observed and modeled signatures was made using the scatter plots and correlation coefficient (Pearson-r). We calculated annual mean streamflow, annual mean monsoon streamflow, low flows, and high flows. These hydrological signatures represent the distinct phases and patterns of the daily streamflow in a catchment and hence, provide us an in-depth idea of model performance. Additionally, we evaluated three distinct segments of the daily flow duration curve (FDC), which represent specific ranges of the streamflow representing the various regimes. Based on the recommendations of (Yilmaz et al., 2008), we calculated percentage bias in observed vs modeled streamflow for the top 2% flows, representing the peak flows (FHV), the slope of the middle section of FDC (FMS) and bottom 30% flows, representing the low flow regime in the catchment. These evaluations provide us with a granular assessment of model performance across the varying flow conditions. The model performance was also assessed against peak timing error and peak mean absolute percentage error (MAPE). The observed and simulated peaks are calculated using SciPy's standard peak

finding algorithm. For a peak to occur in observed data, the flow must be greater than one standard deviation of historical values, and a corresponding distance of 100 days must be present between two such flows. A corresponding peak in simulated data is defined as the highest flow inside a window of 3 days around the observed peak. The peak timing error corresponds to the average lag in days between simulated and observed peaks, whereas peak MAPE shows the mean absolute percentage error in their magnitude.

Since the LSTM models did not train on the out-of-sample catchment set, we could perform the evaluation on the entire available time series. This ensures strict evaluation of the generalizability of the LSTM models, as there is no possibility of selecting a favorable evaluation period. The figures show in-sample catchments as circles and out-of-sample catchments as triangles, wherever applicable.

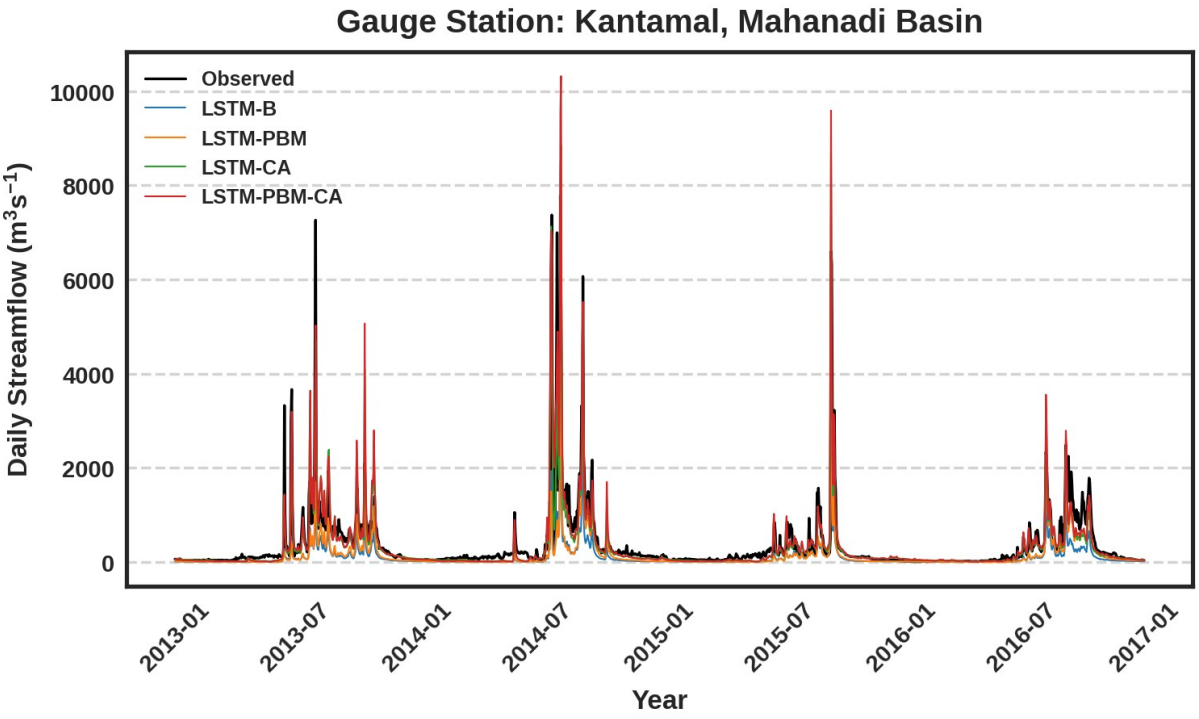

Figure 3. Representative hydrograph plot showing daily streamflow time series of testing period (2013-2016) for a catchment to highlight the agreement between observed and simulated flows by various LSTM models.

3 Results and Discussion

3.1 Performance of physically informed LSTM models

Integrating physically relevant information, such as simulated land surface states and static geophysical catchment attributes, into the LSTM models, could help the models to contextualize the time series data within the larger framework of the underlying physics of the catchment. It enables the LSTM models to benefit from broader datasets, resulting in the improved ability to capture complex interactions, dependencies, and non-linear relationships that may not be evident from time series data alone. Therefore, along with our base LSTM model (LSTM-B), we also trained three additional LSTM models: LSTM-PBM, LSTM-CA and LSTM-PBM+CA (section 2.2.2). Fig.3 shows a daily streamflow time series of a catchment for each model compared against the observed streamflow. While LSTM-B and LSTM-PBM underestimated the flows significantly, the models that were trained on the catchment-specific attributes (LSTM-CA and LSTM-PBM-CA) showed improved ability to simulate the flows with higher accuracy in timing and magnitude.

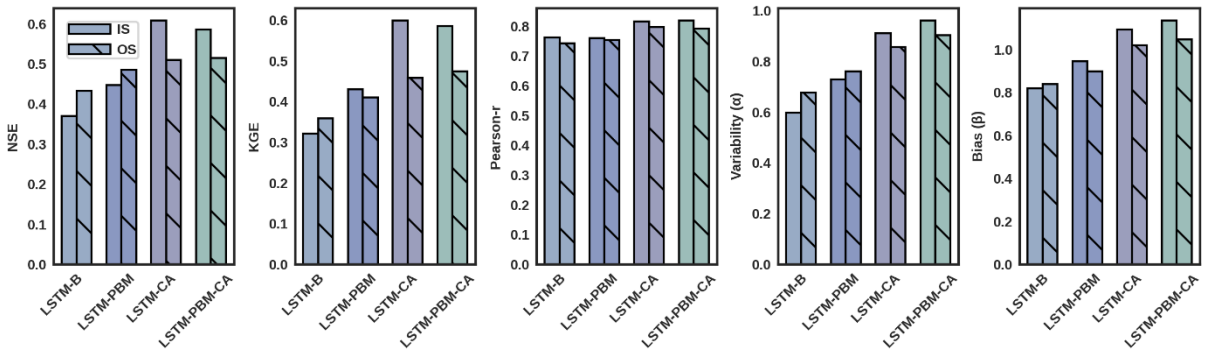

Figure 4. A histogram plot showing the distribution of various error metrics calculated by comparing observed and simulated daily streamflow for in-sample (IS) and out-of-sample (OS) catchments for four models. The numbers on y-axis indicate median values for each metric, and the hatching pattern distinguishes between in-sample and out-of-sample catchments.

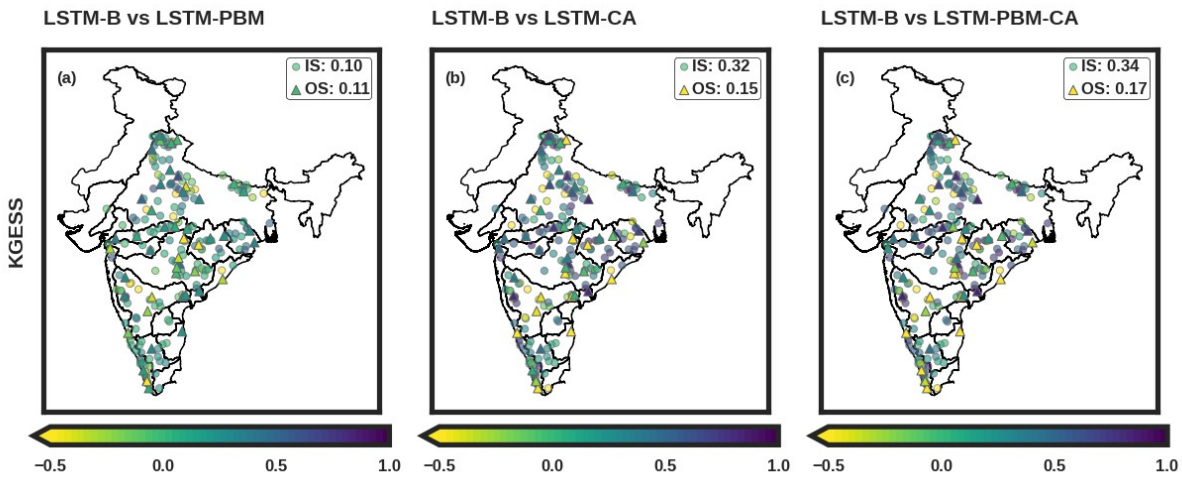

Figure 5. Spatial distribution of KGESS by comparing the KGE for the base model (LSTM-B) with the other three models. The inset value denotes median KGESS for in-sample (IS) and out-of-sample (OS) catchments. The dots represent in-sample catchments while triangles are used to show out-of-sample catchments. The color scale ranges from -0.5 to 1.0 for KGESS value at each point.

Fig.4 shows the progressive gain in skill of the four models using different error metrics. Overall, the LSTM-CA is the best-performing model among all the models that were trained. Our base model, LSTM-B, simultaneously trained on 170 catchments using various meteorological forcing variables to predict one day ahead streamflow. The nationwide median KGE of LSTM-B was a respectable 0.32 and 0.36 for in-sample and out-of-sample catchments, respectively. To evaluate the relative gain in skill, we used KGESS (section 2.3.1), which measures the relative improvement in KGE of the new models in comparison to the base LSTM model. Fig.5 shows the KGESS distribution across in-sample and out-of-sample catchments for LSTM-B vs LSTM-PBM, LSTM-CA and LSTM-PBM-CA, respectively. We observed that passing land surface states as a proxy of catchment hydrological behavior improves the performance by a median KGESS of 0.1 and 0.11 in in-sample and out-of-sample catchments, respectively. This implies that the LSTM models extracted information from land surface states and improved the prediction of streamflow across catchments. Moving on to LSTM-CA, we observe a significant gain in skill by the LSTM with median KGESS of 0.32 and 0.15 in in-

sample and out-of-sample catchments, respectively. We observed that the catchment geophysical attributes provide valuable information to LSTM that helps it to generalize spatial patterns across multiple catchments and allow the model to group similar catchments, and hence provide better streamflow predictions. While we gained overall KGE skill by providing additional information to the LSTM, results also suggest that the performance degraded in a few catchments. Moreover, the highest KGESS was observed in catchments of central and peninsular India, which have complex hydrology due to anthropogenic influences such as agriculture, irrigation, and control structures. The LSTM-PBM-CA was trained on all the available data, including meteorological forcings, static attributes, and simulated land surface states. The KGESS did not see major improvements in LSTM-PBM-CA (Fig.5c), and thus, geophysical attributes proved to be the biggest contributing factor in skill gain.

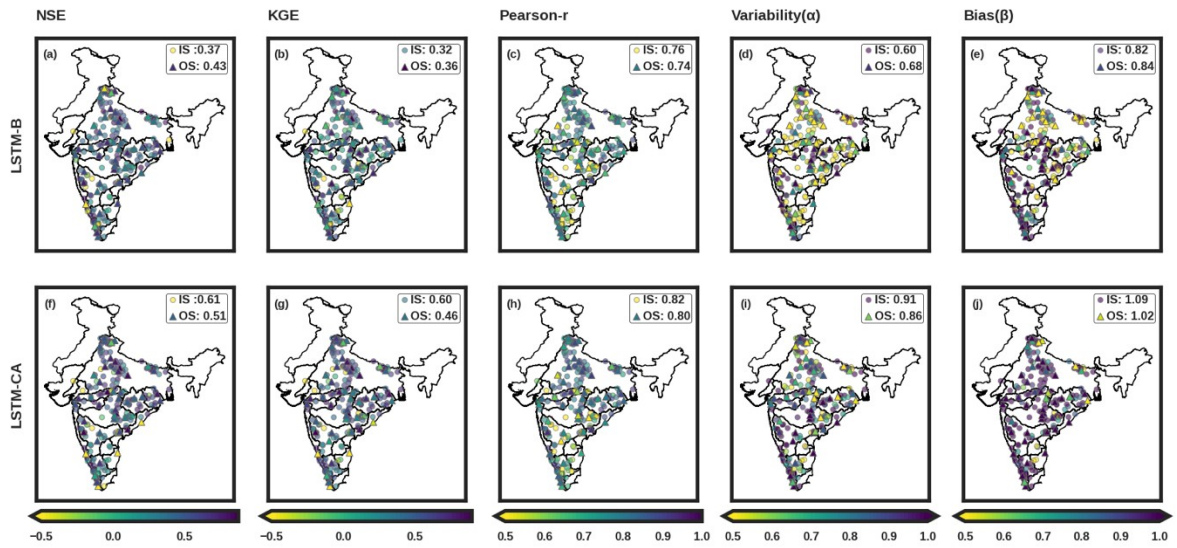

Figure 6. Spatial distribution of error metrics of the base model (LSTM-B) and the best-performing model (LSTM-CA). The inset value denotes the nationwide median of each error metric for in-sample (IS) and out-of-sample (OS) catchments. The dots represent in-sample catchments while triangles are used to show out-of-sample catchments. The color scale range varies as per the error metric displayed.

Fig.6 shows the spatial distribution of various error metrics, highlighting the relative performance of LSTM-B vs LSTM-CA over India. For simplicity, we plot only LSTM-CA as

it has the highest median skill among the three models compared with LSTM-B. The median value of NSE for LSTM-B is 0.37 and 0.43 for the in-sample and out-of-sample catchments, respectively. The NSE performance of LSTM-CA is significantly higher than LSTM-B, with median values of 0.61 and 0.51 in in-sample and out-of-sample catchments, respectively. The distribution of NSE reveals that the catchments further downstream perform poorly compared to the upstream catchments, both in-sample and out-of-sample catchments. This is expected as downstream catchments generally have a higher degree of human influence. Similarly, the nationwide median KGE for LSTM-B is 0.32 and 0.36 in in-sample and out-of-sample catchments, respectively. Again, the KGE performance of LSTM-CA is higher than LSTM-B, with nationwide median values of 0.60 and 0.46 for in-sample and out-of-sample gauges, respectively. We also observe a very slight increase in NSE and KGE performance of LSTM-PBM-CA vs LSTM-CA, hinting that the LSTM-PBM-CA model was positively influenced by the information provided by land surface states as a proxy to underlying physics of the catchment. However, the gain in performance is very minor to support this finding. The correlation coefficient (r), variability ratio (Alpha) and volumetric bias (Beta) show similar gains in the skill of LSTM-CA for in-sample and out-of-sample catchments (Fig.S1). Overall, the LSTM-CA model was most skillful in capturing the dynamics of daily streamflow across the various catchments of India. We also observed that LSTM-PBM-CA scored the highest median coefficient of variation, measured by KGE-α, both in-sample and out-of-sample catchments ranging from 3.5% to 13% improvement over LSTM-CA (Table S3). This indicates that simulated outputs from a physically based model can capture the variance in a better way than standalone models such as LSTM-B or LSTM-CA. However, due to loss in skill for other KGE components in LSTM-PBM-CA, LSTM-CA still stood out as an overall best suitable model for predicting daily streamflow.

We further investigated the performance of models based on the Köppen-Geiger climate classes in India. The overall best performing model, LSTM-CA, scored highest KGE

(0.67) in temperate regions of the country, followed by tropical catchments (0.62) and lowest in arid catchments (0.43), for in-sample catchments. However, we see an increase in skill for LSTM-CA in out-of-sample arid catchments with a median KGE of 0.52. The LSTM-PBM-CA slightly outperforms LSTM-CA in out-of-sample arid and temperate catchments. Our findings match the results of previous studies (see Kratzert et al. 2018), where the authors suggested that LSTM models struggle with zero flows. Additionally, it has been noted in previous studies that non-perennial flow and arid flow conditions result in very little change in observed discharge, making it difficult for models to capture the process in the absence of significant variance. Moreover, it may be possible that our input features lack sufficient representation of the sub-surface flow dynamics, which may be dominant in the drier catchments.

Reservoirs significantly alter the natural dynamics of streamflow in a catchment, posing a challenge to hydrological modelling. To quantify the human influence in the form of reservoir storage on model performance, we classified the catchments into two groups, with and without reservoirs using available public records and satellite imagery (Fig.S2). Fig.7 shows the effect of reservoir storage on the prediction performance of each LSTM variant for in-sample catchments. The catchments where streamflow is heavily influenced by reservoir management perform poorly compared to the catchments where reservoirs are absent. On average, the models outperformed by 55.37% in median KGE for catchments without reservoirs. The highest percentage difference in performance is seen in LSTM variants trained using static catchment attributes. Similar patterns were observed in the out-of-sample catchments (Fig.S3). The increasing practices of flow management and stark differences in model performance enforce the need for measurement and explicit representation of human influences in hydrological modelling.

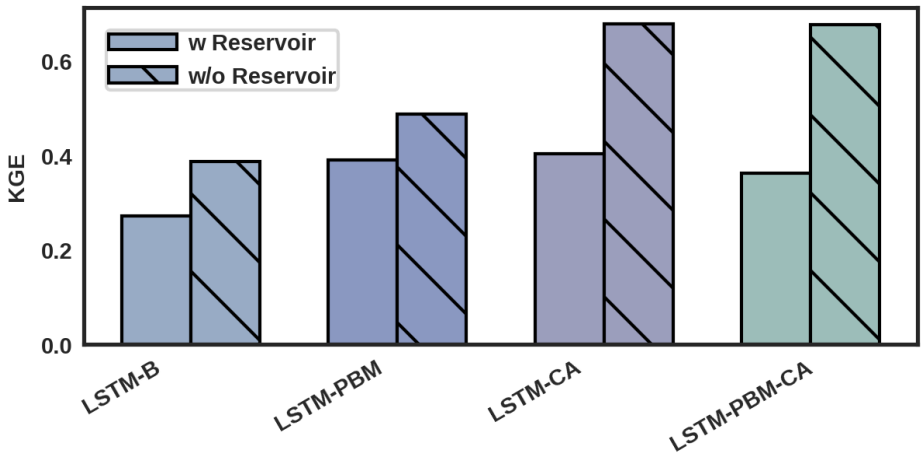

Figure 7. Histogram showing the relative difference in KGE metric for 170 in-sample catchments with (w Reservoir) and without reservoir (w/o Reservoir). All LSTM model variants perform better in catchments without an upstream reservoir.

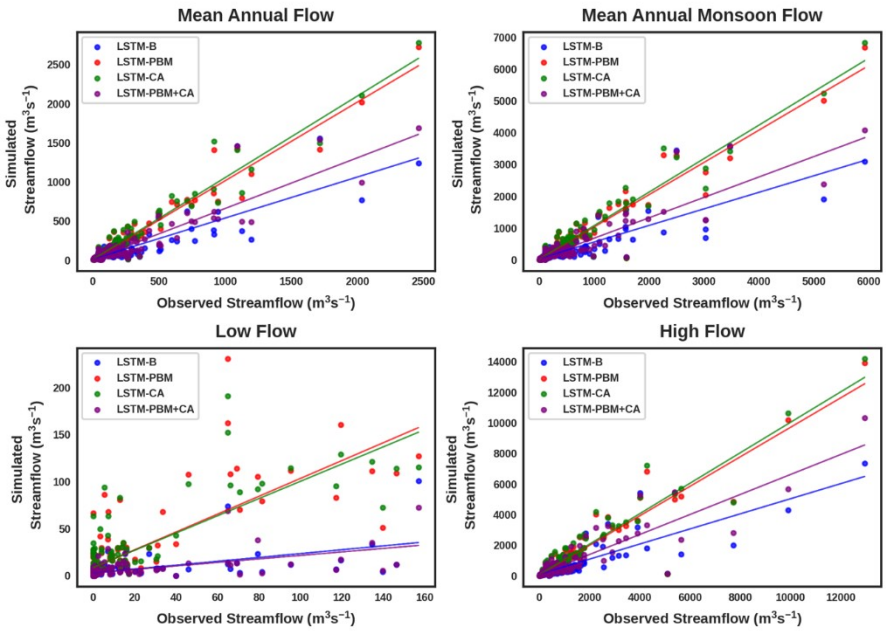

Figure 8. Scatter plot of observed vs simulated hydrological signatures calculated for in-sample catchments for all LSTM variants.

3.2 Evaluation of hydrological signatures

Fig.7 shows the scatter for observed vs simulated hydrological signatures in the in-sample catchments for all LSTM model variants. The mean annual flow is the daily streamflow averaged annually, whereas the mean annual monsoon flow represents the daily streamflow

during the monsoon season that lasts from June to September in India. The low flow represents the daily streamflow that gets exceeded 95% of the days, and the high flow corresponds to the daily streamflow that gets exceeded only 5% of the days. We calculated coefficient of determination (R2) to analyse the relative performance of various models. The models were able to reproduce the hydrological signatures across all the catchments (in-sample and out-of-sample) with high accuracy. However, the models permed poorly in simulating the low flows across India. The LSTM-PBM underestimated the flows in catchments, it performed slightly better in simulating low flows with less bias. However, when the other three signatures are considered, LSTM-CA remains the best-performing model. It may be noted that the performance of LSTM-CA in out-of-sample catchments does not degrade significantly, which indicates that the model was successful in learning the long-term dependencies as well as the similarities among catchments, resulting in a well-generalized performance.

Table 3. A summary of various hydrograph evaluation metrics with nationwide median values. %FHV, % FMS, and %FLV represent bias in high flow volume, mid-section slope and low flow volume of flow duration curve. Peak timing and Peak MAPE represent mean timing and magnitude error in simulating the streamflow peaks. The values are provided separately for in-sample (IS) and out-of-sample (OS) catchments.

Metric	***LSTM***		***LSTM-PBM***		***LSTM-CA***		***LSTM-PBM-CA***	
	IS	***OS***	***IS***	***OS***	***IS***	***OS***	***IS***	***OS***
% bias FHV	-20.43	-18.60	-14.42	-14.08	-6.92	-9.39	-3.42	-7.97
% bias FMS	-14.75	-3.88	-12.72	-7.60	-20.46	-7.02	-16.91	-7.43
% bias FLV	-86.83	-10.80	-63.58	8.96	30.98	32.12	20.36	34.28
Peak Timing (days)	0.94	0.64	0.93	0.65	0.78	0.63	0.80	0.67
Peak MAPE (%)	67.05	64.90	61.75	61.75	47.87	51.79	46.55	52.19

While evaluating the three distinct flow regimes corresponding to each catchment, derived from flow duration curves, we selected % bias to understand the models' performance.

The % bias denotes the relative difference in magnitude of observed and simulated values, expressed as a percentage, providing a negative or positive value. The positive value denotes that the simulated streamflow was higher than observed and vice versa. Table 3 shows the summary of % bias for peak flow volume (FHV), the mid-section slope of FDC (FMS) and low flow volume (FLV) across all the in-sample and out-of-sample catchments for the four models. As observed in low flow hydrological signature (bottom 5%), the FLV (bottom 30%) also exhibit overestimation by the LSTM models, indicating that the low flow regimes are difficult to simulate. It may also be noted that absolute low extremes for many catchments, especially in peninsular regions, were near zero due to non-perennial nature and large human influences. Interestingly, LSTM-PBM-CA gains over LSTM-CA in FLV simulation as opposed to low flow hydrological signature evaluation, which indicates that land surface information in LSTM networks might hold a slight advantage in simulating general low flows other than the absolute extremes (bottom 5% in our case). The other two sections of FDC, namely FHV and FMS, show better performance and lower bias than FLV. The high flow regimes (top 2%) were simulated with a nationwide median negative bias (underestimation) of –6.92% and –3.42% in in-sample catchments by LSTM-CA and LSTM-PBM-CA, respectively. A slightly lower performance (higher underestimation) is observed in FHV for out-of-sample catchments, indicated by median values of –9.39% and –7.97% for LSTM-CA and LSTM-PBM-CA, respectively. We see an even larger underestimation of FMS, as compared to FHV, for LSTM-CA, with a nationwide median of –20.46% and –7.02% for in-sample and out-of-sample catchments, respectively. Once again, LSTM-PBM-CA performs slightly better in matching the magnitudes of FMS with nationwide median % Bias of –16.91% and –7.44% for in-sample and out-of-sample catchments, respectively. Interestingly, the out-of-sample catchments displayed a better median % bias for both LSTM-CA and LSTM-PBM-CA. Overall, the evaluation of FDC suggests that the models simulated with information of underlying hydrological processes, such as represented by land surface states in our case, could

help the LSTM models to perform slightly better over general flow conditions, in contrast to flow extremes. The assessment of peak timing error and peak MAPE suggest that LSTM-CA and LSTM-PBM-CA performed equally well compared to LSTM-B. The mean peak timing error reduced from 0.94 (0.64) days in LSTM-B to 0.78 (0.63) and 0.8 (0.67) in in-sample (out-of-sample) catchments for LSTM-CA and LSTM-PBM-CA, respectively. Correspondingly, peak MAPE reduced from 67.05% in LSTM-PB to 47% and 46% in in-sample catchments for LSTM-CA and LSTM-PBM-CA, respectively.

3.3 Discussion

In this study, we found that incorporating catchment geophysical attributes into the training of LSTM networks significantly enhances their predictability, aligning with findings from previous global studies. These static catchment properties, along with a large number of training samples, enable LSTM networks to internally classify homogeneous catchments and efficiently transfer learned parameters across catchments (Biswal et al., 2024). Additionally, this approach helps LSTM networks manage the non-homogeneity in training periods across different gauge locations in our study, which often arises from varying length of observation records. While the land surface model outputs were less effective in improving LSTM performance for in-sample catchments, they provided marginal improvement in out-of-sample catchments with a gain of 13% in KGESS over LSTM-CA (Fig.5). This outcome confirms our hypothesis that physically based model outputs help constrain LSTM parameters in out-of-sample (ungauged) catchments. The information gain is relatively minimal for in-sample catchments where LSTM networks have already extracted the intrinsic relations from existing observed data. We also found that catchments with upstream reservoirs posed training challenges, leading to lower performance, suggesting that anthropogenic influences on streamflow management are difficult to model and predict accurately.

This study extends the work of few previous studies and explores applicability of large sample data driven modelling on hydrologically diverse catchments across India. Previously, Mangukiya et al. (2023) showed that a single LSTM model trained on 55 catchments performed better than individual LSTM networks for each catchment, and observed that the performance suffers in arid regions, which is also confirmed by our findings. At the same time, this study trained on a nationally and climatologically representative 220 catchments, also presents an in-depth analysis of how various sources of physical information contribute to the LSTM modeling skill. The inclusion of the catchments from central India, especially the Ganga River basin, allowed us to provide a more robust LSTM model. A set of previous studies have also explored techniques such as regionalization approaches and empirical methods to predict streamflow in ungauged catchments (Patnaik et al., 2019; Swain and Patra, 2017). These methods, while innovative, have certain limitations, particularly when compared to the deep learning methods such as LSTM networks. Patnaik et al. (2019) introduced a calibration-free model based on an empirically derived 'decay function,' tested on 108 Indian catchments. The authors paired it with Box-Cox transformation on discharge values to assign equal importance high and low flows. While this approach provides a noteworthy improvement in prediction, the reliance on a universal decay function still imposes constraints. These constraints, such as the model's performance variability across different hydrological conditions, particularly during peak flows, highlight the limitations of traditional empirical models when applied to complex, diverse catchments. Swain and Patra (2017) evaluated spatial proximity, regression and physical similarity techniques to calibrate SWAT and predict streamflow in 32 ungauged catchments in India. While Kriging and Inverse Distance Weighted methods showed promise, the presence of a "well-gauged" catchment in proximity to ungauged catchments proved critical. Our approach, utilizing LSTM networks, offers significant advancement over these traditional methods. LSTM networks are designed to capture complex temporal dependencies and non-linear relationships inherent in hydrological data. They can learn directly from raw

data, without the need for manual feature extraction or reliance on regionalization, thus providing a more flexible and scalable solution. This positions our method as a more robust and versatile tool for hydrological prediction, especially in ungauged catchments and large-scale multi-basin scenarios, where traditional methods face significant challenges.

One of the limitations of this study is that the catchment attributes such as vegetation type and land use/land cover are not considered as dynamic variables, resulting in a static representation of human influence in ever-changing catchment behavior (Ye et al., 2003, 2013). Future studies could incorporate these dynamic effects using improved observation data such as satellite images and in-situ records. Additionally, multiple studies have emphasized a need for interpretability of machine learning and an active effort towards process understanding in such models. Istalkar et al. (2023) demonstrated that understanding of the process that governs the target variable can help design the inputs in an informed manner, resulting in an improved predictability of DL models. Beven (2020) addresses the challenges in using DL models for hydrological modelling, focusing on inconsistencies in input data, interpretation of processes, and inclusion of process information and local uniqueness. He states that if the objective is hydrological prediction, improving process information and data consistency is considered sufficient, which we have tried to address in our study. One of the future works could be to derive inferences from DL which could involve extracting information from DL's internal states or parameters as one of the approaches, leading the researchers towards interpretable machine learning models.

4 Conclusions

This study explores the applicability of LSTM networks to model rainfall-runoff dynamics over tropical regions such as India, with an emphasis on the role of additional physical information in improving the accuracy of streamflow predictions. The complex topography and extensive water management practices in the Indian subcontinent present a challenging

environment for hydrologists to accurately predict streamflow. We evaluated the relative advantages of incorporating various types of hydrologically relevant data to train the LSTM networks. In each model, we incrementally added additional information and assessed the skill of each model with respect to the base LSTM model. The results were evaluated using multiple error metrics, hydrological signatures, flow duration curves and flow extremes. The major findings of the study are the following:

- Including geophysical information in the LSTM models improves the national median KGE from 0.32 to 0.60 and 0.36 to 0.46 for in-sample and out-of-sample catchments, respectively. Static catchment attributes led to a greater improvement compared to simulated land surface states, with 80% of the in-sample catchments showing improved KGE.
- The model performance was 55.37% higher in terms of median KGE in catchments without reservoirs, indicating that water management practices are hard to capture without explicit representation in the training data.
- The arid catchments were found difficult to model with an average degradation of 32% in median KGE compared to temperate and tropical catchments for best-performing model.
- The best performing LSTM variant, i.e., LSTM trained with geophysical catchment attributes, retained 77% of prediction skill in terms of median KGE, for 50 out-of-sample catchments, highlighting the ability to leverage large-sample data for a generalized continental-scale streamflow modeling.

Our assessment of LSTM models provides an in-depth insight into the behavior of state-of-the-art deep learning models over the complex hydrological conditions of India. We see a clear advantage of using observable catchment characteristics to improve the streamflow predictions over India using deep learning methods such as LSTM models. The state-of-the-art methods, discussed in this study, can leverage large sample observations and learn complex relationships between various hydrological processes with lower computational complexities compared to physically based models.

Acknowledgements

This research was conducted in the HydroSense lab (https://hydrosense.iitd.ac.in/) of IIT Delhi, and the authors acknowledge the IIT Delhi High-Performance Computing facility for providing computational and storage resources. Dr. Manabendra Saharia gratefully acknowledges financial support for this work through grants from Ministry of Earth Sciences/IITM Pune Monsoon Mission III (RP04574) and Ministry of Earth Sciences (RP04741). The authors gratefully acknowledge the Central Water Commission (CWC), National Water Informatics Centre (NWIC), and the Ministry of Jal Shakti (MoJS) for providing the streamflow datasets used in this study. The authors also acknowledge ISRO NRSC for providing access to 1:50000 LU/LC dataset.

Compliance with Ethical Standards

The authors declare that they have no conflict of interest.

Data Availability Statement.

The datasets used in this study are available from the following sources:

- Streamflow: Central Water Commission, India, and India WRIS, https://indiawris.gov.in/wris/
- IMD precipitation and temperature: https://www.imdpune.gov.in/
- IMDAA forcing: https://rds.ncmrwf.gov.in/
- MERIT DEM: http://hydro.iis.u-tokyo.ac.jp/~yamadai/MERIT_DEM/
- NeuralHydrology: https://github.com/neuralhydrology/neuralhydrology
- MODIS LAI: https://ladsweb.modaps.eosdis.nasa.gov/missions-and-measurements/products/MOD15A2H
- SoilGrids: https://soilgrids.org/
- HiHydroSoil v2.0: https://gee-community-catalog.org/projects/hihydro_soil/
- NRSC LU/LC: https://bhuvan.nrsc.gov.in/
- ERA-5: ECMWF, https://www.ecmwf.int/en/forecasts/datasets/reanalysis-datasets/era5

References

Addor, N., Newman, A.J., Mizukami, N., Clark, M.P., 2017. The CAMELS data set: catchment attributes and meteorology for large-sample studies. Hydrol. Earth Syst. Sci. 21, 5293–5313. https://doi.org/10.5194/hess-21-5293-2017

Arsenault, R., Poulin, A., Côté, P., Brissette, F., 2014. Comparison of Stochastic Optimization Algorithms in Hydrological Model Calibration. J. Hydrol. Eng. 19, 1374–1384. https://doi.org/10.1061/(asce)he.1943-5584.0000938

Bengio, Y., Simard, P., Frasconi, P., 1994. Learning long-term dependencies with gradient descent is difficult. IEEE Trans. Neural Netw. Publ. IEEE Neural Netw. Counc. 5, 157–66. https://doi.org/10.1109/72.279181

Beven, K., 2020. Deep learning, hydrological processes and the uniqueness of place. Hydrol. Process. 34, 3608–3613. https://doi.org/10.1002/hyp.13805

Biswal, B., Istalkar, P., Kadu, A., 2024. Troubles in the Paradise: Hydrology Does not Respond to Newtonian Mechanics and the Rise of Machines. pp. 17–25. https://doi.org/10.1007/978-981-97-1227-4_2

Burnash, R.J.C., Ferral, R.L., McGuire, R.A., 1973. A Generalized Streamflow Simulation System: Conceptual Modeling for Digital Computers. U.S. Department of Commerce, National Weather Service, and State of California, Department of Water Resources.

Chakraborty, A., Saharia, M., Chakma, S., Kumar Pandey, D., Niranjan Kumar, K., Thakur, P.K., Kumar, S., Getirana, A., 2024. Improved soil moisture estimation and detection of irrigation signal by incorporating SMAP soil moisture into the Indian Land Data Assimilation System (ILDAS). J. Hydrol. 638, 131581. https://doi.org/10.1016/j.jhydrol.2024.131581

Chang, L.-C., Chang, F.-J., Chiang, Y.-M., 2003. A two-step-ahead recurrent neural network for stream-flow forecasting. Hydrol. Process. 18, 81–92. https://doi.org/10.1002/hyp.1313

Coulibaly, P., Anctil, F., Rasmussen, P., Bobée, B., 2000. A recurrent neural network approach using indices of low-frequency climatic variability to forecast regional annual runoff. Hydrol. Process. - HYDROL PROCESS 14, 2755–2777. https://doi.org/10.1002/1099-1085(20001030)14:153.3.CO;2-0

Devia, G.K., Ganasri, B.P., Dwarakish, G.S., 2015. A Review on Hydrological Models. Aquat. Procedia, INTERNATIONAL CONFERENCE ON WATER RESOURCES, COASTAL AND OCEAN ENGINEERING (ICWRCOE'15) 4, 1001–1007. https://doi.org/10.1016/j.aqpro.2015.02.126

Ek, M.B., Mitchell, K.E., Lin, Y., Rogers, E., Grunmann, P., Koren, V., Gayno, G., Tarpley, J.D., 2003. Implementation of Noah land surface model advances in the National Centers for Environmental Prediction operational mesoscale Eta model. J. Geophys. Res. Atmospheres 108. https://doi.org/10.1029/2002JD003296

Fang, K., Shen, C., 2020. Near-Real-Time Forecast of Satellite-Based Soil Moisture Using Long Short-Term Memory with an Adaptive Data Integration Kernel. J. Hydrometeorol. 21, 399–413. https://doi.org/10.1175/JHM-D-19-0169.1

Govindaraju, R.S., 2000. Artificial Neural Networks in Hydrology. II: Hydrologic Applications. J. Hydrol. Eng. 5, 124–137. https://doi.org/10.1061/(ASCE)1084-0699(2000)5:2(124)

Hengl, T., Mendes de Jesus, J., Heuvelink, G.B.M., Ruiperez Gonzalez, M., Kilibarda, M., Blagotić, A., Shangguan, W., Wright, M.N., Geng, X., Bauer-Marschallinger, B., Guevara, M.A., Vargas, R., MacMillan, R.A., Batjes, N.H., Leenaars, J.G.B., Ribeiro, E., Wheeler, I., Mantel, S., Kempen, B., 2017. SoilGrids250m: Global gridded soil information based on machine learning. PLOS ONE 12, e0169748. https://doi.org/10.1371/journal.pone.0169748

Hersbach, H., Bell, B., Berrisford, P., Hirahara, S., Horányi, A., Muñoz-Sabater, J., Nicolas, J., Peubey, C., Radu, R., Schepers, D., Simmons, A., Soci, C., Abdalla, S., Abellan, X., Balsamo, G., Bechtold, P., Biavati, G., Bidlot, J., Bonavita, M., De Chiara, G., Dahlgren, P., Dee, D., Diamantakis, M., Dragani, R., Flemming, J., Forbes, R., Fuentes, M., Geer, A., Haimberger, L., Healy, S., Hogan, R.J., Hólm, E., Janisková, M., Keeley, S., Laloyaux, P., Lopez, P., Lupu, C., Radnoti, G., de Rosnay, P., Rozum, I., Vamborg, F., Villaume, S., Thépaut, J.-N., 2020. The ERA5 global reanalysis. Q. J. R. Meteorol. Soc. 146, 1999–2049. https://doi.org/10.1002/qj.3803

Hestness, J., Narang, S., Ardalani, N., Diamos, G., Jun, H., Kianinejad, H., Patwary, M.M.A., Yang, Y., Zhou, Y., 2017. Deep Learning Scaling is Predictable, Empirically.

Hirpa, F.A., Salamon, P., Beck, H.E., Lorini, V., Alfieri, L., Zsoter, E., Dadson, S.J., 2018. Calibration of the Global Flood Awareness System (GloFAS) using daily streamflow data. J. Hydrol. 566, 595–606. https://doi.org/10.1016/j.jhydrol.2018.09.052

Hochreiter, S., Schmidhuber, J., 1997. Long Short-Term Memory. Neural Comput. 9, 1735–1780. https://doi.org/10.1162/neco.1997.9.8.1735

Hsu, K., Gupta, H.V., Sorooshian, S., 1995. Artificial Neural Network Modeling of the Rainfall-Runoff Process. Water Resour. Res. 31, 2517–2530. https://doi.org/10.1029/95WR01955

Istalkar, P., Kadu, A., Biswal, B., 2023. Value of process understanding in the era of machine learning: A case for recession flow prediction. J. Hydrol. 626, 130350. https://doi.org/10.1016/j.jhydrol.2023.130350

Kao, I.-F., Zhou, Y., Chang, L.-C., Chang, F.-J., 2020. Exploring a Long Short-Term Memory based Encoder-Decoder framework for multi-step-ahead flood forecasting. J. Hydrol. 583, 124631. https://doi.org/10.1016/j.jhydrol.2020.124631

Khatun, A., Chatterjee, C., Sahu, G., Sahoo, B., 2023. A novel smoothing-based long short-term memory framework for short-to medium-range flood forecasting. Hydrol. Sci. J. 68, 488–506. https://doi.org/10.1080/02626667.2023.2173012

Kingma, D.P., Ba, J., 2017. Adam: A Method for Stochastic Optimization. https://doi.org/10.48550/arXiv.1412.6980

Kratzert, F., Gauch, M., Klotz, D., Nearing, G., 2024. HESS Opinions: Never train an LSTM on a single basin. https://doi.org/10.5194/hess-2023-275

Kratzert, F., Gauch, M., Nearing, G., Klotz, D., 2022. NeuralHydrology --- A Python library for Deep Learning research in hydrology. J. Open Source Softw. 7, 4050. https://doi.org/10.21105/joss.04050

Kratzert, F., Klotz, D., Brenner, C., Schulz, K., Herrnegger, M., 2018. Rainfall–runoff modelling using Long Short-Term Memory (LSTM) networks. Hydrol. Earth Syst. Sci. 22, 6005–6022. https://doi.org/10.5194/hess-22-6005-2018

Kratzert, F., Klotz, D., Herrnegger, M., Sampson, A.K., Hochreiter, S., Nearing, G.S., 2019. Toward Improved Predictions in Ungauged Basins: Exploiting the Power of Machine Learning. Water Resour. Res. 55, 11344–11354. https://doi.org/10.1029/2019WR026065

Lawrence, D.M., Fisher, R.A., Koven, C.D., Oleson, K.W., Swenson, S.C., Bonan, G., Collier, N., Ghimire, B., van Kampenhout, L., Kennedy, D., Kluzek, E., Lawrence, P.J., Li, F., Li, H., Lombardozzi, D., Riley, W.J., Sacks, W.J., Shi, M., Vertenstein, M., Wieder, W.R., Xu, C., Ali, A.A., Badger, A.M., Bisht, G., van den Broeke, M., Brunke, M.A., Burns, S.P., Buzan, J., Clark, M., Craig, A., Dahlin, K., Drewniak, B., Fisher, J.B., Flanner, M., Fox, A.M., Gentine, P., Hoffman, F., Keppel-Aleks, G., Knox, R., Kumar, S., Lenaerts, J., Leung, L.R., Lipscomb, W.H., Lu, Y., Pandey, A., Pelletier, J.D., Perket, J., Randerson, J.T., Ricciuto, D.M., Sanderson, B.M., Slater, A., Subin, Z.M., Tang, J., Thomas, R.Q., Val Martin, M., Zeng, X., 2019. The Community Land Model Version 5: Description of New Features, Benchmarking, and Impact of Forcing Uncertainty. J. Adv. Model. Earth Syst. 11, 4245–4287. https://doi.org/10.1029/2018MS001583

Lees, T., Buechel, M., Anderson, B., Slater, L., Reece, S., Coxon, G., Dadson, S.J., 2021. Benchmarking data-driven rainfall–runoff models in Great Britain: a comparison of long short-term memory (LSTM)-based models with four lumped conceptual models. Hydrol. Earth Syst. Sci. 25, 5517–5534. https://doi.org/10.5194/hess-25-5517-2021

Liang, X., Lettenmaier, D.P., Wood, E.F., Burges, S.J., 1994. A simple hydrologically based model of land surface water and energy fluxes for general circulation models. J. Geophys. Res. Atmospheres 99, 14415–14428. https://doi.org/10.1029/94JD00483

Magotra, B., Prakash, V., Saharia, M., Getirana, A., 2022. Towards an Indian Land Data Assimilation System for Water Resources Applications 2022, H21D-03.

Mangukiya, N.K., Sharma, A., Shen, C., 2023. How to enhance hydrological predictions in hydrologically distinct watersheds of the Indian subcontinent? Hydrol. Process. 37, e14936. https://doi.org/10.1002/hyp.14936

Minns, A.W., Hall, M.J., 1996. Artificial neural networks as rainfall-runoff models. Hydrol. Sci. J. 41, 399–417. https://doi.org/10.1080/02626669609491511

Myneni, Ranga, Knyazikhin, Yuri, Park, Taejin, 2021. MODIS/Terra Leaf Area Index/FPAR 8-Day L4 Global 500m SIN Grid V061. https://doi.org/10.5067/MODIS/MOD15A2H.061

Nearing, G.S., Kratzert, F., Sampson, A.K., Pelissier, C.S., Klotz, D., Frame, J.M., Prieto, C., Gupta, H.V., 2021. What Role Does Hydrological Science Play in the Age of Machine Learning? Water Resour. Res. 57, e2020WR028091. https://doi.org/10.1029/2020WR028091

Ni, L., Wang, D., Singh, V.P., Wu, J., Wang, Y., Tao, Y., Zhang, J., 2020. Streamflow and rainfall forecasting by two long short-term memory-based models. J. Hydrol. 583, 124296. https://doi.org/10.1016/j.jhydrol.2019.124296

Niu, G.Y., Yang, Z.L., Mitchell, K.E., Chen, F., Ek, M.B., Barlage, M., Kumar, A., Manning, K., Niyogi, D., Rosero, E., Tewari, M., Xia, Y., 2011. The community Noah land surface model with multiparameterization options (Noah-MP): 1. Model description and evaluation with local-scale measurements. J. Geophys. Res. Atmospheres 116. https://doi.org/10.1029/2010JD015139

Pai, D.S., Sridhar, L., Rajeevan, M., Sreejith, O.P., Satbhai, N.S., Mukhopadhyay, B., 2014. Development of a new high spatial resolution (0.25× 0.25) long period (1901–2010) daily gridded rainfall data set over India and its comparison with existing data sets over the region. Mausam 65, 1–18.

Parlos, A., Rais, O., Atiya, A., 2000. Multi-step-ahead Prediction Using Dynamic Recurrent Neural Networks. Neural Netw. 13, 765–786. https://doi.org/10.1016/S0893-6080(00)00048-4

Patnaik, S., Sharma, V.C., Biswal, B., 2019. Evaluation of an instantaneous dryness index-based calibration-free continuous hydrological model in India. Hydrol. Res. 50, 915–924. https://doi.org/10.2166/nh.2019.081

Rani, S.I., T, A., George, J.P., Rajagopal, E.N., Renshaw, R., Maycock, A., Barker, D.M., Rajeevan, M., 2021. IMDAA: High Resolution Satellite-era Reanalysis for the Indian Monsoon Region. J. Clim. 1–78. https://doi.org/10.1175/JCLI-D-20-0412.1

Rumelhart, D.E., Hinton, G.E., Williams, R.J., 1986. Learning representations by back-propagating errors. Nature 323, 533–536. https://doi.org/10.1038/323533a0

Sahoo, B.B., Jha, R., Singh, A., Kumar, D., 2019. Long short-term memory (LSTM) recurrent neural network for low-flow hydrological time series forecasting. Acta Geophys. 67, 1471–1481. https://doi.org/10.1007/s11600-019-00330-1

Solomatine, D.P., Ostfeld, A., 2008. Data-driven modelling: some past experiences and new approaches. J. Hydroinformatics 10, 3–22. https://doi.org/10.2166/hydro.2008.015

Srivastava, A.K., Rajeevan, M., Kshirsagar, S.R., 2009. Development of a high resolution daily gridded temperature data set (1969–2005) for the Indian region. Atmospheric Sci. Lett. 10, 249–254.

Swain, J.B., Patra, K.C., 2017. Streamflow estimation in ungauged catchments using regionalization techniques. J. Hydrol. 554, 420–433. https://doi.org/10.1016/j.jhydrol.2017.08.054

Wang, L., Mao, S., Wilamowski, B., 2019. Short-Term Load Forecasting with LSTM Based Ensemble Learning. 2019 Int. Conf. Internet Things IThings IEEE Green Comput. Commun. GreenCom IEEE Cyber Phys. Soc. Comput. CPSCom IEEE Smart Data SmartData 793–800. https://doi.org/10.1109/iThings/GreenCom/CPSCom/SmartData.2019.00145

Xiang, Z., Yan, J., Demir, I., 2020. A Rainfall-Runoff Model With LSTM-Based Sequence-to-Sequence Learning. Water Resour. Res. 56. https://doi.org/10.1029/2019WR025326

Yamazaki, D., Ikeshima, D., Tawatari, R., Yamaguchi, T., O'Loughlin, F., Neal, J.C., Sampson, C.C., Kanae, S., Bates, P.D., 2017. A high-accuracy map of global terrain elevations. Geophys. Res. Lett. 44, 5844–5853. https://doi.org/10.1002/2017GL072874

Ye, B., Yang, D., Kane, D.L., 2003. Changes in Lena River streamflow hydrology: Human impacts versus natural variations. Water Resour. Res. 39. https://doi.org/10.1029/2003WR001991

Ye, X., Zhang, Q., Liu, J., Li, X., Xu, C., 2013. Distinguishing the relative impacts of climate change and human activities on variation of streamflow in the Poyang Lake catchment, China. J. Hydrol. 494, 83–95. https://doi.org/10.1016/j.jhydrol.2013.04.036

Yeditha, P.K., Rathinasamy, M., Neelamsetty, S.S., Bhattacharya, B., Agarwal, A., 2021. Investigation of satellite precipitation product driven rainfall-runoff model using deep learning approaches in two different catchments of India. J. Hydroinformatics 24, 16–37. https://doi.org/10.2166/hydro.2021.067

Yilmaz, K.K., Gupta, H.V., Wagener, T., 2008. A process-based diagnostic approach to model evaluation: Application to the NWS distributed hydrologic model. Water Resour. Res. 44. https://doi.org/10.1029/2007WR006716

Young, P.C., Beven, K.J., 1994. Data-based mechanistic modelling and the rainfall-flow non-linearity. Environmetrics 5, 335–363. https://doi.org/10.1002/env.3170050311

Yucel, I., Onen, A., Yilmaz, K.K., Gochis, D.J., 2015. Calibration and evaluation of a flood forecasting system: Utility of numerical weather prediction model, data assimilation

and satellite-based rainfall. J. Hydrol. 523, 49–66.
https://doi.org/10.1016/j.jhydrol.2015.01.042

Annexure 1. A list of all the features used for training the LSTM models to predict daily streamflow.

	Feature	Source	Details
Hydrological and Meteorological Inputs			
1	Precipitation	IMD	0.25° Daily
2	Maximum Air Temperature	IMD	1° Daily
3	Minimum Air Temperature	IMD	1° Daily
4	Relative Humidity	IMDAA	0.12° Hourly
5	Surface Pressure	IMDAA	0.12° Hourly
6	Downward Shortwave Radiation	IMDAA	0.12° Hourly
7	Downward Longwave Radiation	IMDAA	0.12° Hourly
8	Soil Moisture	Noah-MP3.6	0.1° Daily
9	Baseflow	Noah-MP3.6	0.1° Daily
10	Surface Runoff	Noah-MP3.6	0.1° Daily
Catchment Geophysical Inputs			
11	Area	Shapefiles	-
12	Mean Elevation	MERIT DEM	90m Resolution
13	Mean Slope	MERIT DEM	90m Resolution

14	Mean Annual Precipitation	IMD	0.25° Daily
15	Mean Annual PET	ERA5	0.25° Daily
16	Aridity	Calculated using (14,15)	-
17	High Precip. Frequency (days)	IMD	0.25° Daily
18	Low Precip. Frequency (days)	IMD	0.25° Daily
19	Soil Hydraulic Conductivity	HiHydroSoil v2.0	250-m Global
20	Soil Porosity	HiHydroSoil v2.0	250-m Global
21	Clay Fraction	SoilGrids	250-m Global
22	Silt Fraction	SoilGrids	250-m Global
23	Sand Fraction	SoilGrids	250-m Global
24	Maximum Leaf Area Index	MODIS LAI	0.5° 8-Day
25	Difference in Leaf Area Index	MODIS LAI	0.5° 8-Day
26	Built-up Fraction	NRSC LU/LC	56m
27	Forest Fraction	NRSC LU/LC	56m
28	Crop Land Fraction	NRSC LU/LC	56m
29	Waterbody Fraction	NRSC LU/LC	56m

IMD: Indian Meteorological Department; IMDAA: Indian Monsoon Data Assimilation and Analysis; MERIT DEM: Multi-Error-Removed Improved-Terrain DEM; MODIS LAI: Moderate Resolution Imaging Spectroradiometer Leaf Area Index; NRSC LU/LC: National Remote Sensing Centre Land/Use Land Cover

Supplementary File

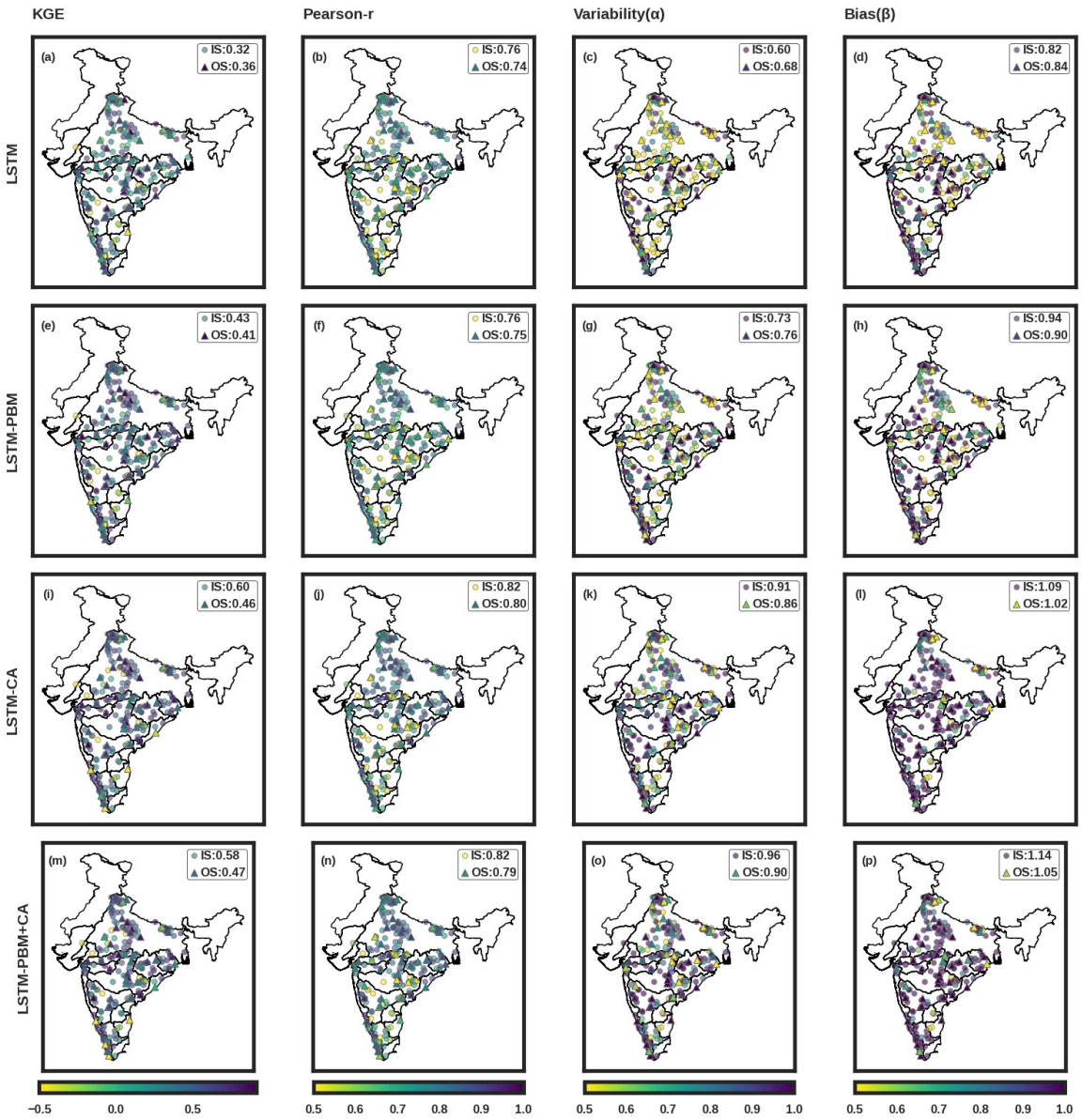

Fig. S1 A composite plot showing spatial distribution of various error metrics for all variants of LSTM model

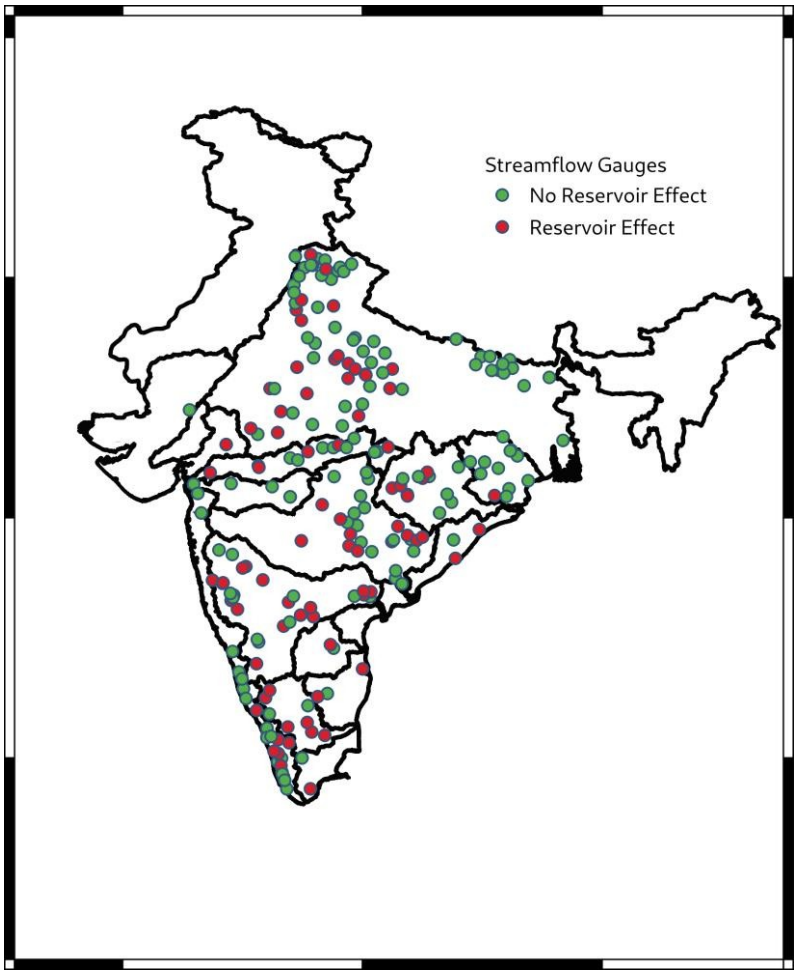

Fig. S2 A map showing the classfication of gauge stations based on presence of an upstream reservoir.

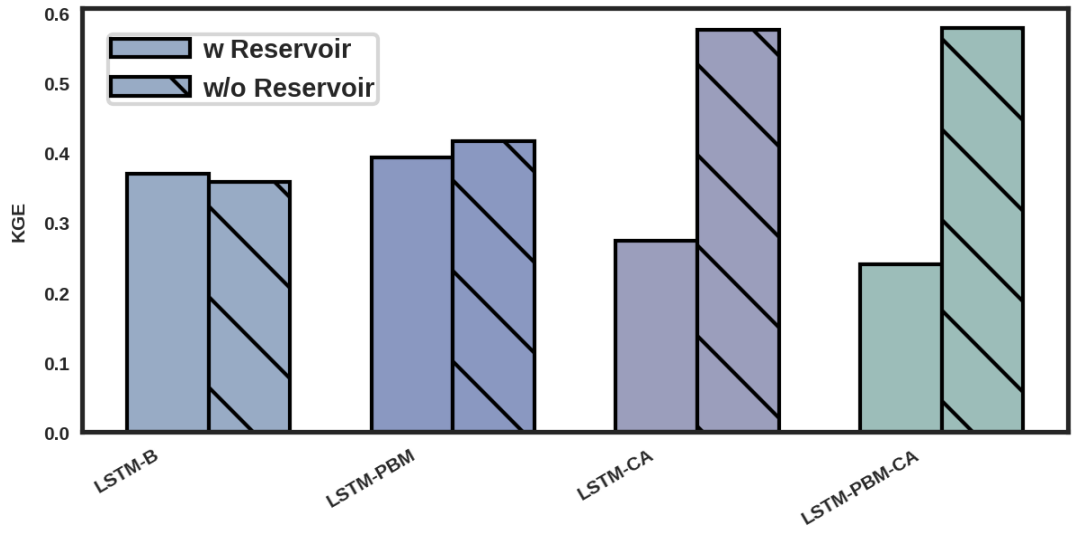

Fig. S3 A histogram showing the difference in KGE for out-of-sample catchments having upstream reservoir versus no reservoir.